ISSN 1028-334X, Doklady Earth Sciences, 2024, Vol. 514, Part 1, pp. 29–37. © Pleiades Publishing, Ltd., 2024.
ISSN 1028-334X, Doklady Earth Sciences, 2024. © Pleiades Publishing, Ltd., 2024.

GEOLOGY

Tectonic Displacements of the Nansen Basin Sedimentary Cover: Causes and Consequences

S. Yu. Sokolov[a,*], G. D. Agranov[a,b], V. A. Kulikov[c], A. V. Zayonchek[a], and A. L. Grokholsky[b]

Presented by Academician K.E. Degtyarev August 16, 2023

Received August 16, 2023; revised August 20, 2023; accepted August 30, 2023

Abstract—It is established that faults in the sedimentary cover of the Nansen basin and seismic anomalies of the “flat spot” type, associated with methane accumulation, are grouped into three spatial combinations: (1) synchronized faults and spots, (2) spots without faults, and (3) faults without spots. They are generally distributed between the C20 and C12 linear magnetic anomalies over negative variations of the lithosphere density with depths up to ~25–30 km and lateral periodicity ~50 km. Combination 1 originates from serpentinization of the upper mantle rocks in the presence of water penetrating deeply through previously formed tectonic displacements, an increase in the rock volume, and local rise of crystalline blocks, leading to the formation of faults of reverse-fault kinematics, which involves the entire sedimentary cover from the acoustic basement to the ocean bottom. The combination 2 is characterized by predomination of “flat spots” of fluid origin in the absence of faults, which, because of rare seismic observations, may be missed and not appear in a plane of the sections. Combination 3 represents faults without “flat spots” with a spatial step of ~10 km above the acoustic basement highs. In the Bouguer anomalies, this combination is manifested over ~80-km depression of ~25 mGal depth, comparable to the gravity depth under the axis of Gakkel Ridge. This is not due to the linear structure of the ridge, but, perhaps, to a single upper mantle plume. Therefore, the mechanism of the fault formation above it is related not to serpentinization, but to the rise of plume to the surface. Physical modeling of the structure formation during slowdown of the spreading rate, which occurred in the range C20–C12, showed that the amplitude of differences in the basement elevations increases greatly. Comparison with a real acoustic basement shows the similarity of its relief in the corresponding time intervals of the spreading slowdown with the areas of relief change in the physical model. An increase in the amplitudes of the basement highs occurs most likely due to the formation of faults that provide circulation of water necessary for serpentinization.

Keywords: Nansen Basin, sedimentary cover faults, “flat spots,” serpentinization, density section, spreading rates slowdown, physical modeling

DOI: 10.1134/S1028334X23602213

INTRODUCTION

In the western part of the Russian sector of the Nansen Basin adjacent to Franz Josef Land archipelago, several seismic sections were carried out as part of the Arctic-2011 project [1, 15] (Fig. 1). These data, together with Russian and foreign seismic data, formed the basis for an adjusted seismic stratigraphic model of the deep part of the Arctic [6]. Numerous “flat spot”-type anomalies are observed in seismic data of the area studied. The anomalies are interpreted as reservoir-type methane accumulations resulting from serpentinization of rocks in the upper mantle [3] and from the interaction of released hydrogen with dissolved CO_2 in water entering the crystalline part of the crust and the upper mantle along a fault system [7]. These anomalies are usually associated with vertical tectonic faults in the sedimentary cover that involve the entire thickness of sediments from the surface to the acoustic basement highs (Fig. 2), over which they are manifested. The fluid origin of the "flat spots” is confirmed by downward deflection of reflectors in the sedimentary cover beneath this type of anomalies.

[a] *Geological Institute, Russian Academy of Sciences, Moscow, Russia*
[b] *Moscow State University, Earth Science Museum, Moscow, Russia*
[c] *Moscow State University, Geological Faculty, Moscow, Russia*
**e-mail: sysokolov@yandex.ru*

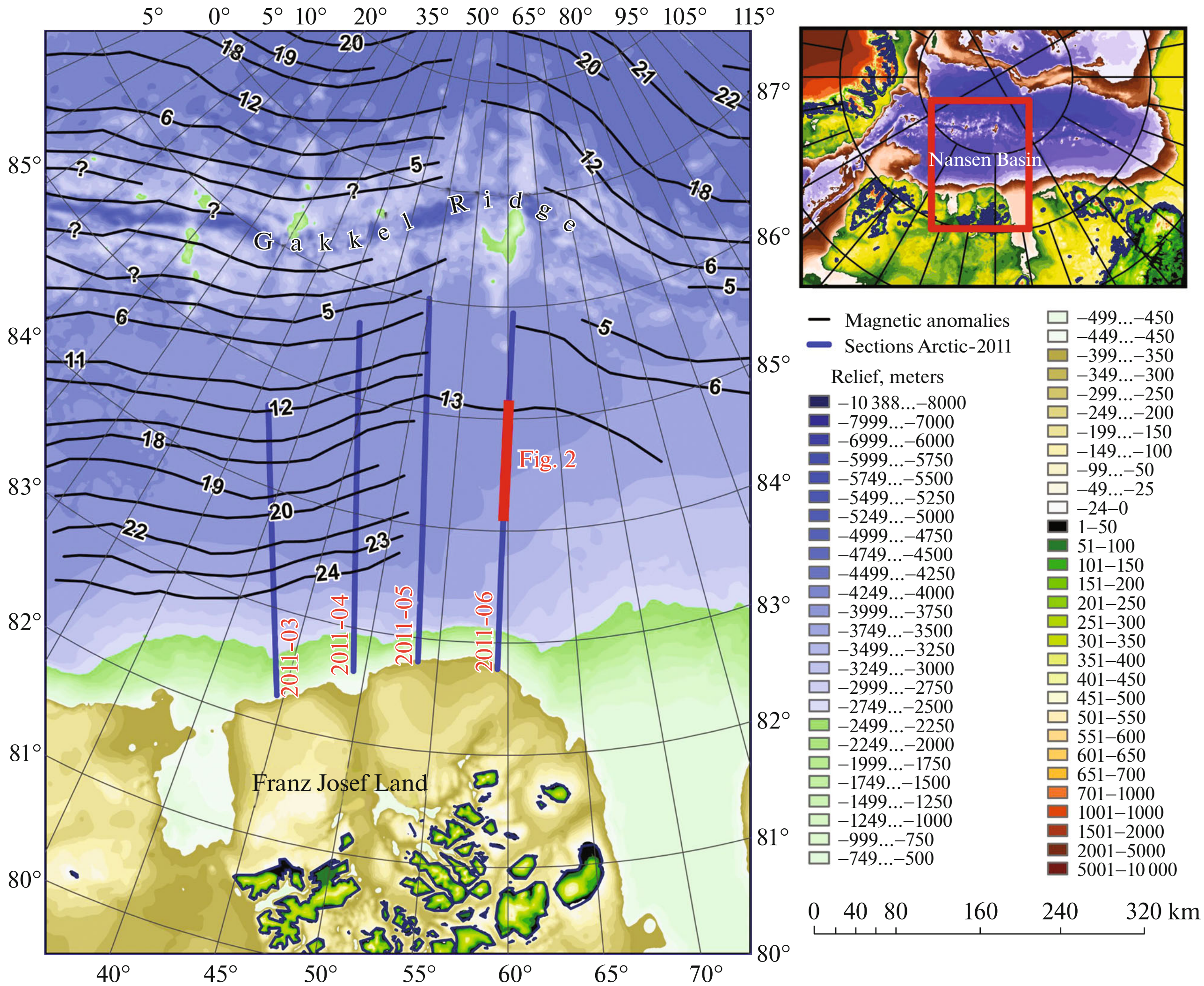

Fig. 1. Seismic sections under the Arctic-2011 project [1, 19] in the western part of the Russian sector of the Nansen Basin. The axes of linear magnetic anomalies are given according to [16]. The red line shows the position of a fragment of the seismic section in Fig. 2.

The purpose of this work is to determine the genesis of tectonic dislocations, analyzing the gravity field in order to identify density heterogeneities in the crust and upper mantle. The density heterogeneities can cause vertical isostatic adjustment of the crust and, consequently, disturbance of the Cenozoic sedimentary cover accumulated on the basement. A significant changes in the topography of the basement in the Eurasian basin is correlated with the linear magnetic anomalies (LMAs) C21, C20 and C13 [15]. “Flat spots” and faults in the section of the studied seismic profiles are located predominantly between the LMAs C20 and C12 [7]. The first stage of the spreading rate slowdown and the formation of higher amplitude relief of the basement occurred in the interval between these anomalies [4]. Therefore, we will compare the identified features of the seismic sections with the distribution of spreading rates in the Nansen Basin and with the results of physical modeling of the structure formation under the slowdown of spreading processes.

Intraplate phenomena in the basins, associated with tectonic activation of the areas without manifestations of the main active geodynamic processes, usually observed at plate boundaries, are of fundamental interest in terms of the stratified and block structure of the oceanic lithospheric plates [9]. In the absence of active factors, the structure of basins should be a stagnant object, where the sedimentary cover is accumulated on the spreading basement with background oceanographic processes affecting the transportation of sediments. Intraplate processes in the basins develop in the presence of off-axis magmatism, or when serpentinization develops along the existing fault network, which can be activated by variations in the tectonic regime parameters.

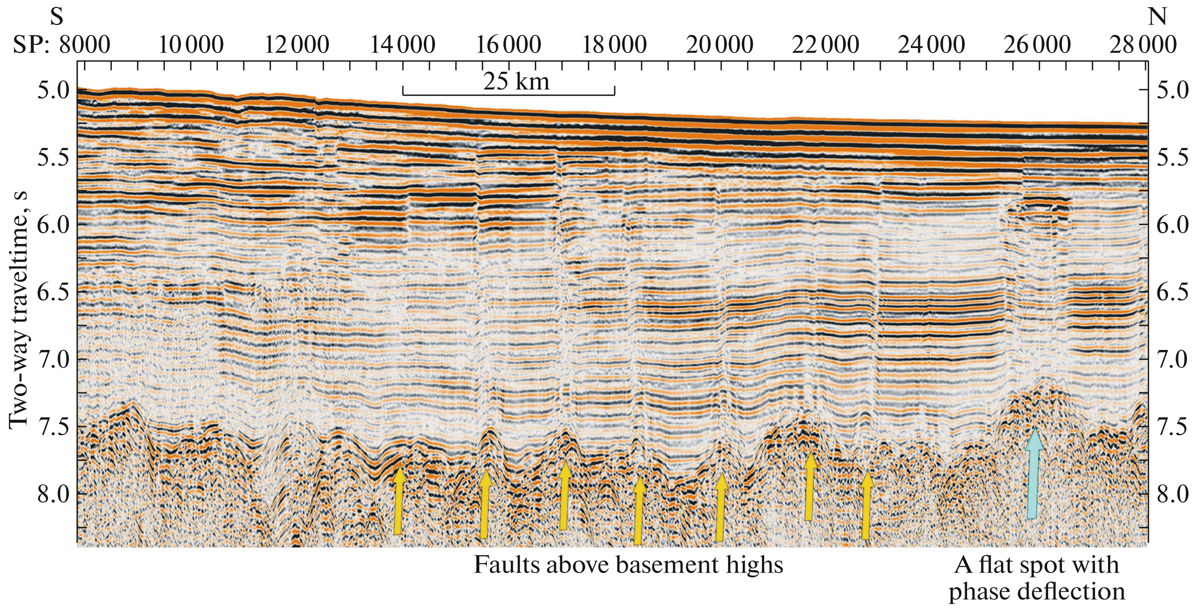

Fig. 2. A fragment of the Arktika-2011-06 section. Yellow arrows show the position of acoustic basement highs under faults in the sedimentary cover. The blue arrow shows the broad highs of the basement beneath a flat spot with reflector deflection in the sedimentary cover. The position of the fragment is shown in Fig. 1.

DATA AND METHODS

The solution of these problems is based on the interpretation of a wave field of the seismic lines of the Arctic-2011 project [1, 15]. In addition to the stratigraphic reference of the main reflectors of the basin section, this study focuses on section elements such as "flat spots" and tectonic dislocations of the sedimentary cover. The picking of these objects in the interpretation software forms a specific database that makes it possible to map their spatial distribution. The "flat spot" anomalies, formed by the accumulation of free gas beneath a local near-surface fluid trap, were interpreted previously [7] (Fig. 3). In the present work, the map compilation is supplemented by the distinguished tectonic displacements in the sedimentary cover of the basin (Fig. 3).

Serpentinization leads to the formation of methane and occurs with the deconsolidation of rocks up to 20% and with the similar increase in volume with vertical movements of crustal blocks. The possibility of serpentinization was proved in [7] by solving a forward gravity model with the addition of similar bodies in the upper mantle for the fit of the observed and calculated anomalous fields. The thickness of the crystalline part of the crust was assumed to be at 4000 m. An unbalanced density source of vertical movements, associated with the increase in the volume of the upper mantle rocks during serpentinization, has been revealed. This source triggers an isostatic response with the formation of dislocations in the sedimentary cover covering the basement. Due to the fact that the top of the second oceanic layer in the seismic lines of the Arctic-2011 project is an acoustic basement and the deeper reflections that could set the geometry for density variations are not traceable, it has been decided to calculate the gravity inversion for the Bouguer reduction without any spatial regularization.

The Bouguer anomalies were calculated based on 2500 m gird the Arctic Gravity project [12] and smoothed in 10-km floating window the IBCAO v.3 grid [14] to the state at which the amplitude spatial spectrum of the topography become comparable to the gravity field spectrum. The density values used were as follows: water 1.03 g/cm^3, continental crust 2.67 g/cm^3, and oceanic crust 2.8 g/cm^3. The result of the calculation is shown as a topographic base in Fig. 3. The same figure shows the profiles along which the inversion was calculated. The edge parts of the profiles are prolonged with entering the shelf and crossing the Gakkel Ridge axis, which is wider than the limits of the seismic data demonstrated in Fig. 3. The calculation was performed in ZondGM2D software [5] using the deconvolution methods and Newton's method with focusing regularization. A vertical grid was formed with a scale factor of 1.2, which, at a starting depth of 1 km, allowed us to form a grid with a depth of up to 100 km on 18 nodes. Figure 4 illustrates the calculated density variations over the four profiles.

The "flat spots" and faults are manifested between LMAs C20 and C12 above the basement, which formed under the conditions of slowing spreading. Therefore, to reveal the features of the structure formation of the consolidated crust, we performed physical modeling of this geodynamic regime for the two-

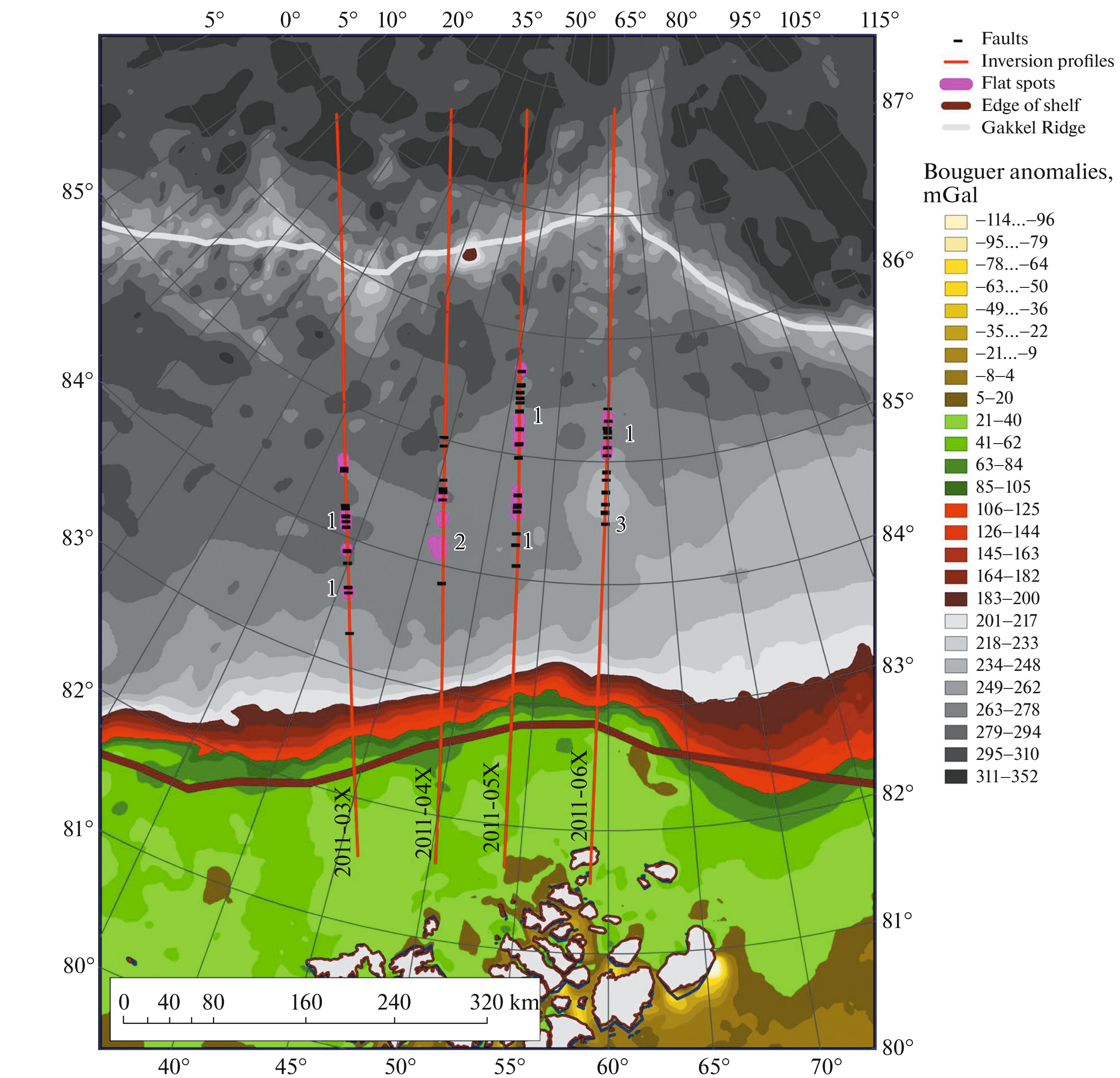

Fig. 3. The spatial distribution of the faults identified from seismic data and the "flat spot" anomalies according to [7]. Bouguer anomalies were calculated from Arctic Gravity Project data [12] on a 2500-m grid using IBCAO v.3 [14]. Red lines show the profiles, along which the gravity field inversion was calculated (Fig. 4). The profiles were drawn along the position of the seismic sections (Fig. 1) with continuation to the shelf and to the intersection with Gakkel Ridge. Numbers indicate the spatial combinations of anomalies and faults observed on the sections: 1, faults in combination with flat spots; 2, flat spots without faults; 3, faults without flat spots.

stage rate reduction (Fig. 5). According to [4], the indicated time interval in the acoustic basement topography along the Arctic-2011-3 section is manifested by typical high-amplitude forms, occupying an intermediate hypsometric position between the basement topography older than the C20–C12 interval with a relatively high spreading rate and younger, but with ultra-slow values. This circumstance creates prerequisites for the modeling performed.

Experimental studies were carried out in the Laboratory of Experimental Geodynamics, Museum of Earth Science, Moscow State University, in accordance with the conditions of similarity and methods described in [2, 19]. On the basis of the experiments on extension of a two-layer model of the lithosphere, these methods propose a model of the formation of relief and normal faults on the ridges with a slow or ultraslow rate of extension. The model material is a complex colloidal system, based on liquid (mineral

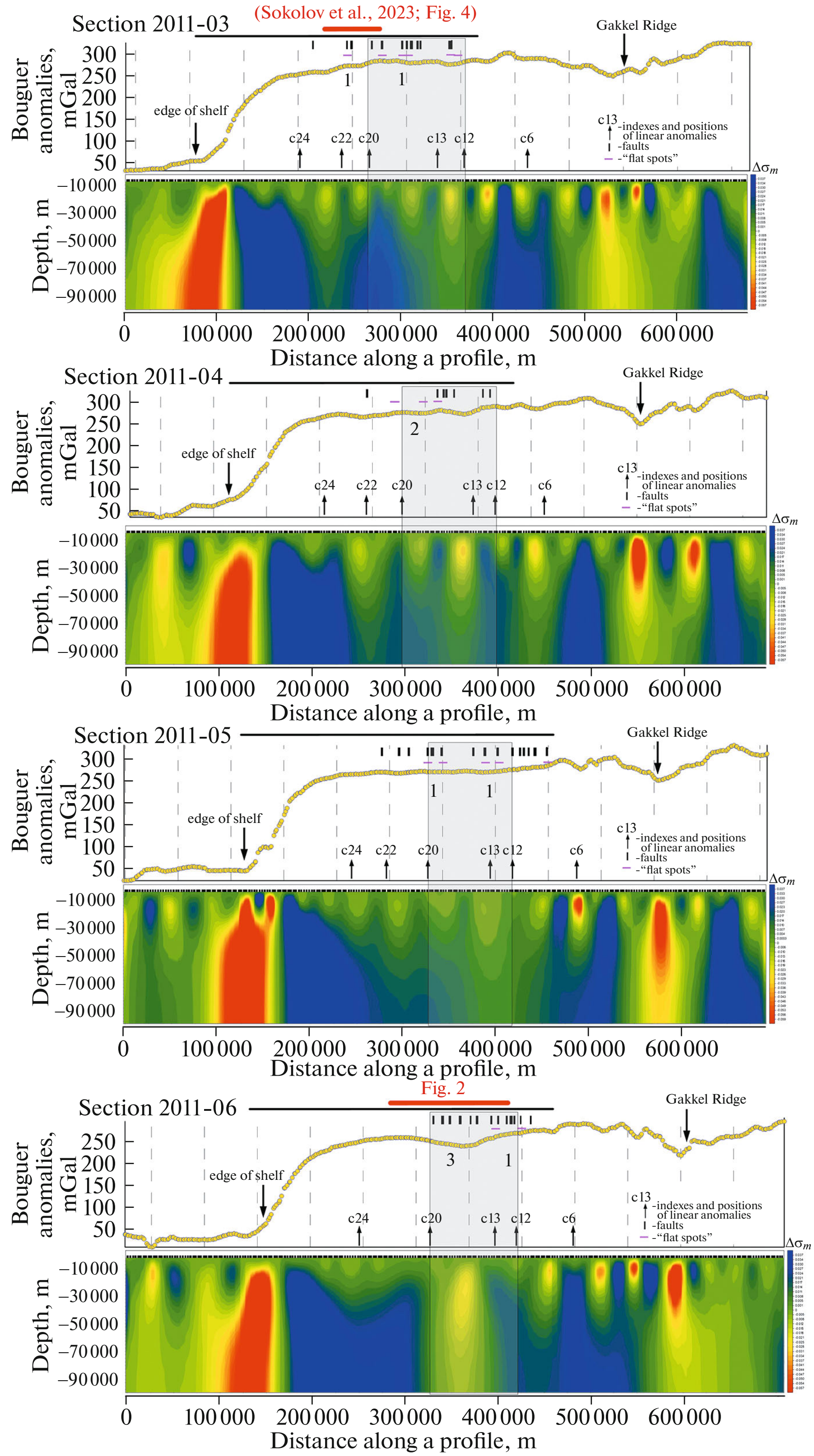

Fig. 4. Calculation of the gravity field inversion along the seismic sections of Arctic-2011 3, 4, 5, 6 (Fig. 1) along the prolonged profiles, the position of which is indicated in Fig. 3. The calculation was performed in the ZondGM2D software [5]. The density variation sections show intersections with linear magnetic anomalies according to [16], faults, and flat spots. Red lines show the positions of the section fragment in Fig. 2 and [7, Fig. 4]. The numbers 1, 2, and 3 indicate the combinations of anomalies and faults from the map (Fig. 3). Gray rectangles show the areas between LMAs C20 and C12.

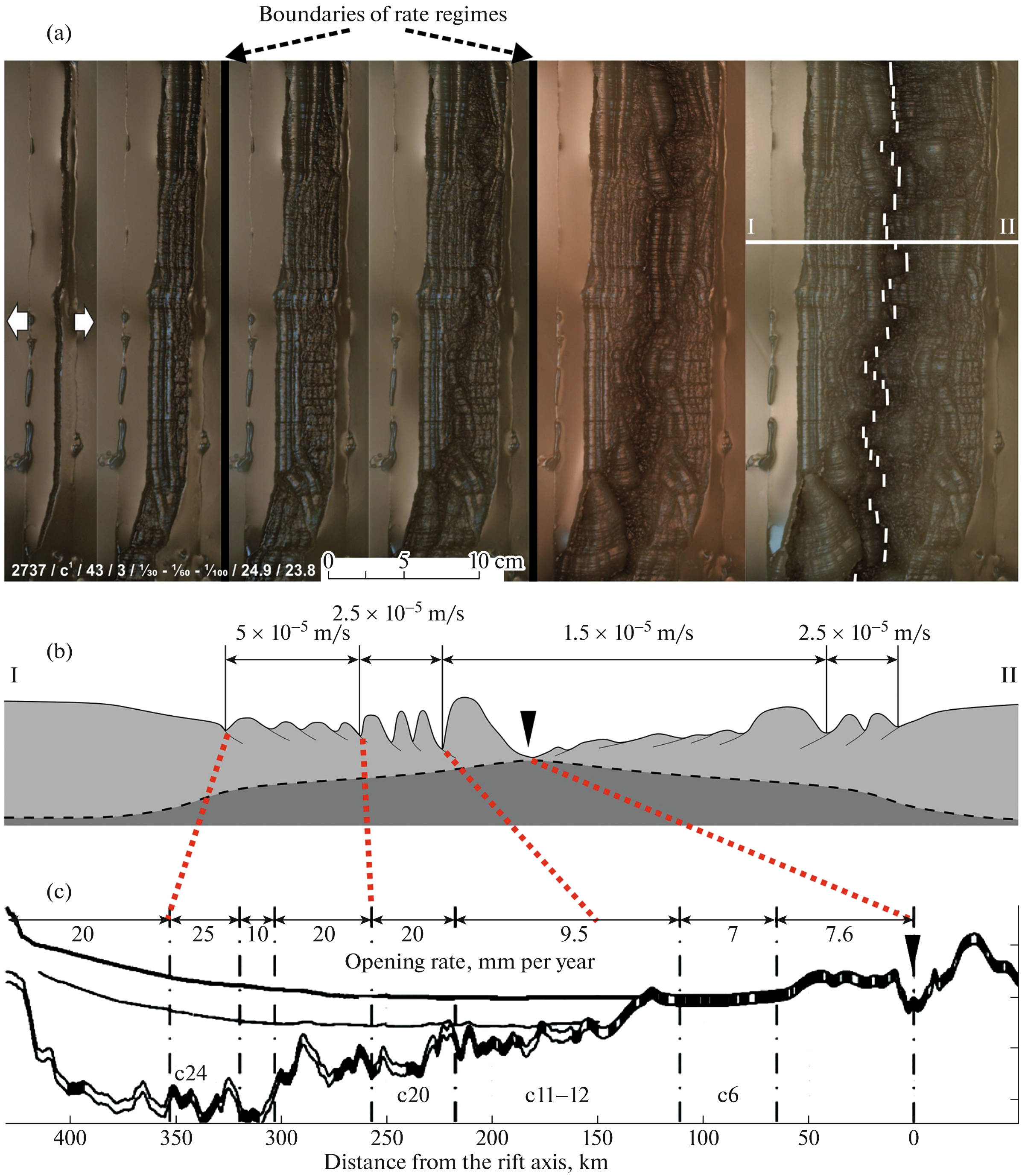

Fig. 5. Features of the structure formation on the southern flank of Gakkel Ridge at two-stage deceleration of the spreading rate according to the data of physical modeling (experiment no. 2737). (a) The step-by-step photographs of structures of the modeled rift in the direction of extension orthogonal to the primary weakened zone; (b) the schematic section of the formed relief along line I–II with indication of the rates in the physical model; (c) comparison of the relief section with the results of identification of magnetic anomalies for the Arktika-2011-3 profile, the basement relief and determination of the spreading rates according to [4].

oil) and solid (ceresin, paraffin) hydrocarbons with various surface-active additives. The material satisfies the similarity criterion in the shear modulus [10]. Meeting the criterion requires that the ratio of stresses in the lithosphere, which caused its deformations (suprahydrostatic stresses), to hydrostatic stresses in the slab has to be the same in nature and in the model. With a stepwise reduction of the spreading rate by a ratio of 2 and 1.6 carried out in the modeling (Fig. 5a), relief with a typical structural pattern was obtained (Fig. 5b). The relief was compared with the real acoustic basement (Fig. 5c).

RESULTS AND DISCUSSIONS

As a result of the cartographic compilation of faults and “flat spot” anomalies (Fig. 3), three spatial combinations of these elements of the seismic sections of the sedimentary cover are determined. The most common combination is the spatial synchronization of the faults and spots (Fig. 3, item 1). The obvious interpretation of the synchronization is formulated on the basis of the solution of the forward gravity model [7] and represents serpentinization of the upper mantle rocks in the presence of water that penetrated into the depths through the previously formed tectonic dislocations, an increase in the volume of rocks, and local rise of crystalline blocks, leading to the formation of faults of reverse-fault kinematics, involving the entire sedimentary cover from the acoustic basement to the bottom surface (Fig. 2). Methane, a product of interaction between CO_2 and hydrogen dissolved in water, is also released along these faults [3]. Getting into the stability zone of gas hydrates, methane transforms into this aggregate state and forms itself a fluid trap, under which it continues to accumulate. This is indicated by similar values of the top depths of the “flat spots,” 390 ± 75 m in all sections analyzed [7], which approximately correspond to the theoretical thickness of the stability zone in the deep-water Arctic [20]. The absence of spots above the basement younger than C12 is explained by the reduction of the sedimentary cover, where they can form. The absence of spots above the basement older than C20 is explained by the possible migration of fluids to the continental slope.

Combination 1 (Fig. 3, item 1), distributed mostly between LMAs C20 and C12, is located above the negative density variations on all sections (Fig. 4) with depths up to ~25–30 km. This value is of the same order of magnitude as the serpentinization depth determined in the basin southwest of the Zonda Trough by the absence of seismicity in the upper mantle [17] due to the more ductile state of the rocks. A more interesting fact is the ~50 km lateral periodicity of negative density variations. With an average spreading rate of ~10 mm/year in the specified time interval [4], it turns out that the formation of the lithosphere is accompanied by such density anomalies every ~5 Ma. A possible interpretation of this density periodicity may be the effect of variable geodynamic activity on the spreading parameters. It is known [8] that the intensity of tectonic processes in the zone of oceanic rifting directly affects the fluctuations in the sea level. The power spectrum of an eustatic curve [13] is characterized by maximum periods of ~5 Ma. In spite of the fact that the Eurasian Basin became connected with the World Ocean only ~18 Ma ago, the planetary periodicity of the sea level fluctuations depends on the planetary geodynamic processes that should be manifested in the Arctic during rifting at Gakkel Ridge regardless of the presence or absence of a water bridge between the ocean basins. This is also confirmed by the character of the change in the spreading rate in the Nansen Basin with a period of ~5 Ma according to [1].

Combination 2 (Fig. 3, item 2) represents the predomination of “flat spots” in the absence of faults. Its interpretation can be the following. According to [1] in the Arctic-2011-4 seismic line, the anomalies contain the reflector deflection beneath them, which clearly indicates their fluid origin. In addition, these anomalies are located above the broad (20 to 30 km) highs of the acoustic basement, with a large height difference (600 and 900 ms) and indicate their association with crustal (and mantle) structures. The absence of visible displacements of reflectors along faults within these anomalies of the Arctic-2011-4 section most likely indicates that the faults may be outside of profile. Taking into consideration that the step between the transects is 50 to 80 km (Fig. 1), fault skipping is quite realistic. A “flat spot” is more difficult to miss, because fluid after migration upward through the section is distributed under a fluid trap and creates anomalies with a width of 2 to 12 km [7]. Fluid migration toward the continental slope from the fault zones cannot be excluded in the presence of a small gradient of near-surface reflectors.

Combination 3 (Fig. 3, item 3) is unique in terms of seismic data and represents the faults without “flat spots.” They represent (Fig. 2) a spatial series of displacements with a spacing of ~10 km, located above acoustic basement highs. The highs rise into the near-surface layers near the bottom above the level of the “flat spot” 490 ms under the bottom in the northern part of the section fragment, which is outside this series of displacements. In the Bouguer anomalies, this series is located above an isometric depression in the values of reduction of ~80 km in diameter (Fig. 3). The difference in values in the center and at the edges of the depression is ~25 mGal, which is comparable to the negative difference of the Bouguer anomalies of ~50 mGal in the Gakkel Ridge axis. These features are clearly visible in the profiles of Fig. 4. The sections along these profiles demonstrate that combination 3 on the Arctic-2011-6 section is located in an area very different from the upper mantle lateral density variations with a step of ~50 km and depths of ~25 km. The character of the density section beneath the area of combination 3 has more similarities with the area of deconsolidation beneath Gakkel Ridge. The fact that a similar deconsolidation in the central part of Nansen Basin is absent on other sections indicates a local rise of the less dense matter. It is related not to the linear structure of the Gakkel Ridge, but possibly to the single upper mantle plume, which is a near-surface branch of another, larger system of heated subvertical channels in the mantle. This is indirectly confirmed by seismic tomography [11]. The data indicate the mantle plume rose from depths of ~550 km on the section through the Nansen Basin east of the Arctic-2011-6 density section. The plume interpretation of the density section suggests the mechanism of fault formation above it, which is associated not with serpentinization and volume increase in the mantle cooled below 500°C, but with the plume rising to the surface in the basin with the sedimentary cover overlying the previously formed spreading basement. The rising plume results in isostatic adjustment of the media with vertical motions of a positive sign.

The time interval C20–C12 is characterized by an approximately twofold decrease in the spreading rate [1, 4] compared to the interval C24–C21. After C20–C12, the spreading rate decreases by another ~1.6 times. Due to the fact that the studied faults and "flat spots" accompanied by negative density variations fell within this interval, the physical modeling of the structure formation was carried out in this geodynamic regime. The experiments showed the following. The ridge relief, formed at the initial stage of extension, has a typical pattern for spreading zones (Fig. 5a). In the area of two-stage rate reduction, the amplitude of the elevation differences increases significantly. For slow-spreading segments of rifts, it is known that high-amplitude basement ridges are usually accompanied by faults going under the Moho boundary [18], along which fluid circulation and serpentinization occur. Further, the significantly asymmetric relief of the basement was formed in the model. The schematic structural profile along the line I–II (Fig. 5b) shows a typical pattern with simple strike–slip structures in the axial zone of the rift and a high probability of transition of the extension axis. This pattern was compared with the real acoustic basement (Fig. 5c) and shows the similarity of its relief heights at the corresponding time intervals with areas of a change in relief in the physical model. The spreading slowdown in two stages causes an increase in the amplitudes of the basement highs in two stages, which is related to the formation of faults under the conditions of low magmatic production typical of slow-spreading ridges. It is also possible that the inertia of the plate motion and the rate of crust formation, leading to torsion of the formed crustal blocks, also come into play depending on the ratio of the drift rate to the rate of magma rise.

CONCLUSIONS

(1) This work studied the faults in the sedimentary cover of the Nansen Basin and "flat spot"-type seismic anomalies in the seismic lines of the Arctic-2011 project. It was found that these elements are grouped into three spatial combinations: 1, synchronized faults and spots; 2, spots without faults; 3, faults without spots.

(2) Interpretation of the origin of combination 1 is serpentinization of the upper mantle rocks in the presence of water that penetrated into the depths through the previously formed tectonic faults, increase in the volume of rocks and local rise of crystalline blocks, leading to the formation of faults of reverse-fault kinematics, involving the entire sedimentary cover from the acoustic basement to the bottom surface. This combination is predominantly distributed between LMAs C20 and C12 over negative density variations with depths up to ~25–30 km and lateral periodicity of ~50 km. This means that, at average spreading rates in the Nansen Basin, such anomalies are formed in the lithosphere every ~5 Ma due to variations in the geodynamic activity.

(3) Combination 2 represents the predomination of "flat spots" in the absence of faults. Interpretation of the origin of these seismic recording anomalies comes to the accumulations of fluids, under which we reveal the reflector deflection and broad, acoustic basement highs with a significant difference in elevation. The faults along which fluids are circulating may be missed due to the sparse observation network and may be outside the section plane. Fluid migration toward the continental slope from fault zones is also not excluded if there is a small gradient of near-surface reflectors.

(4) Combination 3 represents the faults without "flat spots" with ~10 km spacing above acoustic basement highs. In the Bouguer anomalies, this combination on the Arctic-2011-6 seismic line is located above the isometric depression of ~80 km, where the difference in values in the center and at the edges of the depression is ~25 mGal. This is comparable to the negative difference in the Bouguer anomalies due to the ~50 mGal deconsolidation beneath the axis of the Gakkel Ridge and is very different from the upper mantle lateral variations that dominate in the basic data in the Nansen Basin. Similar deconsolidation in the central part of the Nansen Basin is absent on other sections, indicating a localized rise of less dense material. This is not due to the linear structure of Gakkel Ridge, but possibly due to a single upper mantle plume. Thus, the mechanism of the fault formation above t is not related to serpentinization, but to the rise of the plume material to the surface and vertical movements of a positive sign, disturbing the entire sedimentary cover from the spreading basement to the bottom.

(5) The time interval C20–C12 with the main manifestation of faults and spots is characterized by an approximately twofold decrease in the spreading rate. Physical modeling of structure formation under this geodynamic regime has shown that the amplitude of relief gradients strongly increases with a two-stage decrease in the spreading rate. The high-amplitude ridge-like highs of the basement are accompanied by the faults going under the Moho boundary. Fluid circulation and serpentinization occur along these faults. In continuation of the tension, the significantly asymmetric relief of the basement on the tension axis was obtained. Comparison with the real acoustic basement shows the similarity of its relief in the corresponding time intervals of spreading slowdown with the areas of relief change in the physical model. An increase in the amplitudes of the basement highs associated with fault formation is shown.

ACKNOWLEDGMENTS

The authors are grateful to the Russian Federal Geological Foundation (https://rfgf.ru) for access to seismic data and to the Department of Geophysics, Faculty of Geology, Moscow State University, for consultations and the possibility to calculate a gravity field inversion.

FUNDING

This work was supported by Russian Science Foundation, project no. 22-27-00578, "Recent and Modern Geodynamics of the Western Arctic: Evolution and Impact of Active Tectonic Processes on Structural Elements and the Sedimentary Cover of Deep-water Basins and Shelves."

CONFLICT OF INTEREST

The authors declare that they have no conflicts of interest.

REFERENCES

1. *Arctic Basin: Geology and Morphology,* Ed. by V. D. Kaminskii, A. L. Piskarev, and V. A. Poselov (VNIIOkeangeologiya, St. Petersburg, 2017) [in Russian].
2. A. L. Grokhol'skii, E. P. Dubinin, G. D. Agranov, M. S. Baranovskii, Ya. A. Danilov, P. A. Domanskaya, A. A. Maksimova, A. I. Makushkina, A. O. Rashchupkina, A. I. Tolstova, A. N. Filaretova, Yu. A. Sheptalina, and E. L. Shcherbakova, Zhizn' Zemli **42** (4), 485–501 (2020). https://doi.org/10.29003/m1778.0514-7468.2020_42_4/485-501
3. L. V. Dmitriev, B. A. Bazylev, S. A. Silant'ev, M. V. Borisov, S. Yu. Sokolov, and A. Bugo, Ross. Zh. Nauk Zemle **1** (6), 511–519 (1999).
4. A. V. Zaionchek and S. A. Merkur'ev, in *Proc. 24th Int. Sci. Conf. (School) on Marine Geology "Geology of Seas and Oceans*" (Shirshov Institute of Oceanology, Moscow, 2021), Vol. 4, pp. 70–74 [in Russian]. https://doi.org/10.29006/978-5-6045110-7-7
5. A. E. Kaminskii, ZOND Software Package. http://zond-geo.ru.
6. A. M. Nikishin, E. I. Petrov, K. F. Startseva, E. A. Rodina, H. Posamentier, G. Foulger, I. F. Glumov, A. F. Morozov, V. E. Verzhbitskii, N. A. Malyshev, S. I. Freiman, A. P. Afanasenkov, A. V. Bez"yazykov, M. S. Doronina, V. A. Nikishin, S. G. Skolotnev, and A. A. Chernykh, in *Trans. Geol. Inst. Russ. Acad. Sci.* (Geos, Moscow, 2022), Issue 632 [in Russian].
7. S. Yu. Sokolov, W. H. Geissler, A. S. Abramova, D. A. Ryzhova, and I. S. Patina, Lithol. Miner. Resour. **58** (1), 1–15 (2023). https://doi.org/10.1134/S0024490222060074
8. O. G. Sorokhtin and S. A. Ushakov, *The Earth's Evolution* (Moscow State Univ., Moscow, 2002) [in Russian].
9. V. E. Khain and M. G. Lomize, *Geotectonics with Foundations of Geodynamics* (Knizhn. Dom Univ., Moscow, 2005) [in Russian].
10. A. I. Shemenda, Geol. Geofiz., No. 10, 10–19 (1983).
11. A. V. Jakovlev, N. A. Bushenkova, I. Yu. Koulakov, and N. L. Dobretsov, Russ. Geol. Geophys. **53** (10), 963–971 (2012).
12. R. Forsberg and H. Skourup, Geophys. Rev. Lett. **32**, 1–4 (2005).
13. C. G. A. Harrison, Geochem. Geophys. Geosyst. G^3 **3** (8), 1–17 (2002).
14. M. Jakobsson, L. Mayer, B. Coakley, et al., Geophys. Rev. Lett. **39** (12), L12609 (2012).
15. A. M. Nikishin, C. Gaina, E. I. Petrov, et al., Tectonophysics **746** (10), 64–82 (2017).
16. W. Jokat and U. Micksch, Geophys. Rev. Lett. **31**, L02603 (2004). https://doi.org/10.1029/2003GL018352
17. Y. Qin and S. C. Singh, Nat. Commun. **6**, 8298 (2015). https://doi.org/10.1038/ncomms9298
18. A. Rajan, J. Mienert, S. Bunz, and S. Chand, J. Geophys. Res. **117**, B03102 (2012). https://doi.org/10.1029/2011JB008537
19. A. I. Shemenda and A. L. Grocholsky, J. Geophys. Res. **99**, 9137–9153 (1994).
20. K. Wallmann, E. Pinero, E. Burwicz, et al., Energies **5**, 2449–2498 (2012).

Translated by V. Krutikova